© 2016. Published by The Company of Biologists Ltd | Journal of Cell Science (2016) 129, 1234-1249 doi:10.1242/jcs.179382

RESEARCH ARTICLE

A new role for cofilin in retinal neovascularization

Raj Kumar, Jagadeesh Janjanam, Nikhlesh K. Singh and Gadiparthi N. Rao*

ABSTRACT

Pak1 plays an important role in several cellular processes, including cell migration, but its role in pathological angiogenesis is not known. Here, we have determined its role in pathological retinal angiogenesis using an oxygen-induced retinopathy (OIR) model. VEGFA induced phosphorylation of Pak1 and its effector cofilin in a manner that was dependent on time as well as p38MAPKβ (also known as MAPK11) in human retinal microvascular endothelial cells (HRMVECs). Depletion of the levels of any of these molecules inhibited VEGFA-induced HRMVEC F-actin stress fiber formation, migration, proliferation, sprouting and tube formation. In accordance with these observations, hypoxia induced Pak1 and cofilin phosphorylation with p38MAPKβ being downstream to Pak1 and upstream to cofilin in mouse retina. Furthermore, Pak1 deficiency abolished hypoxia-induced p38MAPKβ and cofilin phosphorylation and abrogated retinal endothelial cell proliferation, tip cell formation and neovascularization. In addition, small interfering RNA (siRNA)-mediated downregulation of p38MAPKβ or cofilin levels in the wild-type mouse retina also diminished endothelial cell proliferation, tip cell formation and neovascularization. Taken together, these observations suggest that, although the p38MAPKβ–Pak1–cofilin axis is required for HRMVEC migration, proliferation, sprouting and tubulogenesis, Pak1–p38MAPKβ–cofilin signaling is also essential for hypoxia-induced mouse retinal endothelial cell proliferation, tip cell formation and neovascularization.

KEY WORDS: F-actin, Cofilin, Retinal neovascularization, Sprouting

INTRODUCTION

Angiogenesis is a complex process that requires the coordination of multiple cell types and the activation of different cellular mechanisms (Carmeliet, 2000, 2005). Most importantly, endothelial cells from existing vessels protrude as multicellular sprouts to form new blood vessels (Nguyen et al., 2013). The endothelial cell invasion process is thought to occur over several steps including degradation of extracellular basement membrane that paves the way for endothelial cell migration, sprouting and lumen formation (Yancopoulos et al., 2000). Dysregulation in any of these events can contribute to non-patterning and non-productive vessel formation, which mostly results in pathological angiogenesis (Carmeliet, 2003; Folkman, 1995). Among the numerous factors identified thus far that stimulate both developmental and pathological angiogenesis, VEGFA appears to be the most predominant angiogenic factor (Adams and Alitalo, 2007; Carmeliet, 2000). VEGFA stimulates endothelial cell multiplication, migration and differentiation into tip cells. These tip cells guide the angiogenic sprouts and control the fate of the adjacent cells (Gerhardt et al., 2003). Although VEGFA is a potent angiogenic factor, the mechanisms by which it influences endothelial cell cytoskeleton remodeling and its role in differentiation of endothelial cells into tip cells leading to sprouting are not completely understood.

During the past two decades, work from various laboratories has indicated that the p21-activated kinase (Pak) family of serine/threonine kinases are involved in different cellular processes, including cytoskeleton remodeling and focal adhesion formation leading to cellular migration, proliferation and transcriptional regulation (Kichina et al., 2010). Pak1, which is the major isoform of the group I Paks, and which is activated by GTP bound Rho-GTPases such as Rac1 and Cdc42, has a wide range of tissue distribution, and is overexpressed in different types of cancers (Ong et al., 2013). Some reports have shown that Pak1 signaling plays a role in angiogenesis, as loss of Rac1 and Pak1 function in endothelial cells resulted in impaired lamellipodia and filopodia formation or migration (Kiosses et al., 2002; Ong et al., 2013). Despite these reports implicating a role for Pak1 in angiogenesis, its involvement in retinal neovascularization is not known. Pak1 mediates its effects on cytoskeleton remodeling through phosphorylation and inactivation of cofilin (Delorme et al., 2007). Furthermore, many studies have also demonstrated that, although cofilin inhibition stabilizes F-actin stress fibers, its activation disassembles these F-actin filaments (Breitsprecher et al., 2011; Sumi et al., 1999). Because the Pak1–cofilin axis plays an important role in cytoskeleton remodeling, which is required for both cell migration and proliferation (Ho et al., 2013; Zipfel et al., 2006), in this study we have tested the role of Pak1 and its downstream effector cofilin in VEGFA-induced endothelial cell cytoskeleton remodeling and angiogenic signaling. Here, we report that blocking Pak1 activation diminishes VEGFA-induced human retinal microvascular endothelial cell (HRMVEC) migration, proliferation, sprouting and tube formation *in vitro*. In addition, we demonstrate that Pak1 deficiency reduces mouse retinal endothelial cell proliferation and tip cell formation, thereby reducing the amount of neovascularization in an oxygen-induced retinopathy (OIR) model *in vivo*. Furthermore, our data show that both inactivation and activation of cofilin are essential for F-actin stress fiber formation, migration, DNA synthesis, sprouting and tube formation of HRMVECs *in vitro* and mouse retinal neovascularization *in vivo*. Interestingly, we observed that p38MAPKβ (also known as MAPK11) acts upstream or downstream of Pak1 in endothelial cells of human and mouse origin, respectively, to mediate VEGFA-induced cofilin phosphorylation, cytoskeleton remodeling and angiogenic signaling.

RESULTS

Pak1 mediates VEGFA-induced angiogenic events in HRMVECs

Angiogenesis, which plays an essential role in development, is also an important player in multiple disease processes and is initiated by sprouting of endothelial cells, for which VEGFA is a crucial factor (Carmeliet, 2005). Given that sprouting is a dynamic process in the

Department of Physiology, University of Tennessee Health Science Center, Memphis, TN 38163, USA.

*Author for correspondence (rgadipar@uthsc.edu)

Received 20 August 2015; Accepted 2 February 2016

Journal of Cell Science

Journal of Cell Science (2016) 129, 1234-1249 doi:10.1242/jcs.179382

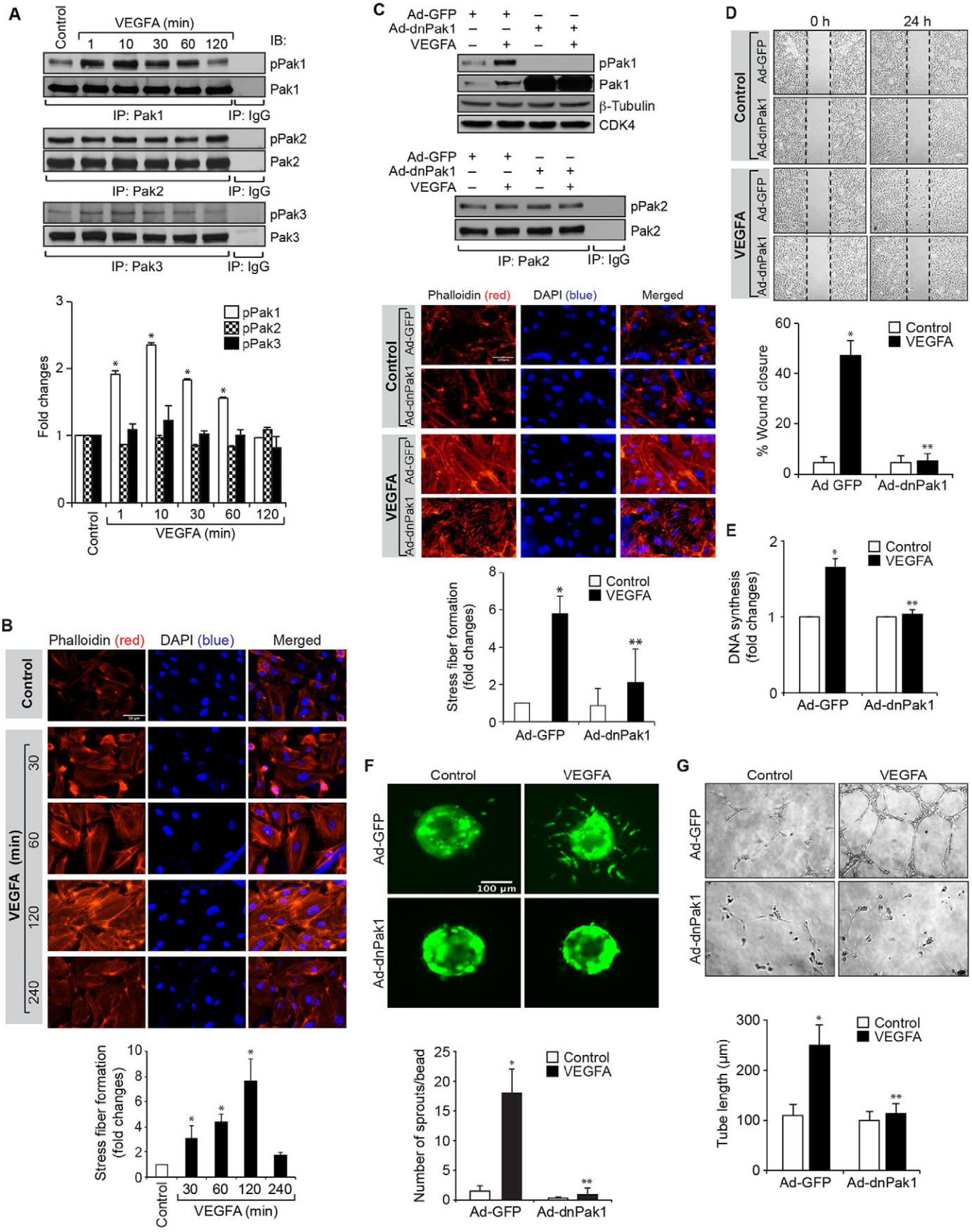

Fig. 1. See next page for legend.

Journal of Cell Science

Journal of Cell Science (2016) 129, 1234-1249 doi:10.1242/jcs.179382

Fig. 1. Pak1 mediates the VEGFA-induced angiogenic events of HRMVECs. (A) Quiescent HRMVECs were treated with and without VEGFA (40 ng/ml) for the indicated time periods and cell extracts were prepared. Equal amounts of protein from control and each treatment were immunoprecipitated (IP) with anti-Pak1, anti-Pak2 or anti-Pak3 antibodies and the immunocomplexes were analyzed by western blotting using antibodies against phosphorylated (p)Pak1, pPak2 or pPak3. Results were normalized to Pak1, Pak2 or Pak3 levels and are presented in the graph. (B) After treating with and without VEGFA (40 ng/ml) for the indicated time periods, cells were stained with Rhodamine-labeled phalloidin to assess F-actin stress fiber formation. The changes in stress fiber levels were assessed by measuring the fluorescence intensity, and are presented as the fold changes relative to control. (C) Cells were transduced with Ad-GFP or Ad-dnPak1 (40 MOI), growth-arrested, and treated with and without VEGFA (40 ng/ml) for 10 min. Cell extracts were prepared and analyzed by western blotting for pPak1 levels using pPak1/2/3 antibody, or immunoprecipitated with anti-Pak2 antibody and the immunocomplexes were analyzed by western blotting for pPak2 levels as described in A. Alternatively, the transduced cells were treated with and without VEGFA (40 ng/ml) for 2 h and examined for F-actin stress fiber formation with phalloidin staining as described in B. The pPak1 blot was reprobed for Pak1, and β-tubulin and CDK4 levels to show the overexpression of the dominant-negative Pak1 and for normalization, respectively. Scale bars: 50 µm. (D–G) All the conditions were the same as in C except that cells were treated with and without VEGFA (40 ng/ml) and subjected to a migration (D), DNA synthesis (E), sprouting (F) or tube formation (G) assay. The bar graphs represent quantitative analysis of three independent experiments. The values represent mean±s.d. **P*<0.01 vs control or Ad-GFP; ***P*<0.01 vs Ad-GFP plus VEGFA (one-way ANOVA followed by Tukey's post-hoc test).

regulation of angiogenesis (Kim et al., 2011), in this study we have investigated its underlying mechanisms. Pak1 plays a crucial role in actin cytoskeleton remodeling, which is essential for both cell migration and proliferation (Dharmawardhane et al., 1997; Ho et al., 2013; Kichina et al., 2010). Therefore, in order to understand the role of Pak1 in VEGFA-induced sprouting, we first analyzed the effect of VEGFA on Pak1 activation. We observed a time-dependent increase in Pak1 T423 phosphorylation upon VEGFA stimulation in HRMVECs with a maximum effect at 10 min (Fig. 1A). VEGFA had no effect on Pak2 or Pak3 phosphorylation, which indicates its specificity for Pak1 activation (Fig. 1A). VEGFA also induced F-actin stress fiber formation in a time-dependent manner with a maximum effect at 2 h (Fig. 1B). To test the role of Pak1 in VEGFA-induced F-actin stress fiber formation, we used a dominant-negative mutant approach. Adenoviral-mediated expression of dominant-negative (dn)Pak1, without having any effect on Pak2 phosphorylation or its steady-state levels, suppressed VEGFA-induced Pak1 phosphorylation (Fig. 1C). Furthermore, blockade of Pak1 activation by use of dnPak1 attenuated VEGFA-induced HRMVEC F-actin stress fiber formation, migration, DNA synthesis, sprouting and tube formation (Fig. 1C–G).

Pak1 deficiency reduces tip cell formation and retinal neovascularization

To extrapolate the significance of the *in vitro* observations on the involvement of Pak1 in VEGFA-induced angiogenic events to the *in vivo* situation, we investigated its role in pathological retinal neovascularization using a mouse model of OIR (Pierce et al., 1995). Pak1$^{-/-}$ mice showed a significantly reduced retinal vasculature and neovascularization as compared to C57BL/6 (WT) mice at postnatal day (P)17 (Fig. 2A–C). As a result of reduced vasculature and neovascularization, Pak1$^{-/-}$ mice exhibited an increased avascular area, suggesting that Pak1 also has a role in retinal vascularization (Fig. 2D). In addition, endothelial cell proliferation as measured by immunofluorescence colocalization of CD31 (also known as PECAM1) and Ki67 was decreased in the retinas of Pak1$^{-/-}$ mice as compared to wild-type (WT) mice (Fig. 2E). We also observed that the retinas from Pak1$^{-/-}$ mice exhibited reduced filopodia projections as compared to the retinas from WT mice, indicating a decrease in tip-cell formation (Fig. 2F), which is consistent with the role of Pak1 in VEGFA-induced sprouting. To assess whether the above-observed effects on reduced retinal neovascularization are intrinsic to retinal endothelial cell loss of Pak1, endothelial cells from WT and Pak1$^{-/-}$ mice retinas were isolated and tested for their capacity to undergo VEGFA-induced sprouting. VEGFA induced sprouting only in WT but not Pak1$^{-/-}$ mice retinal endothelial cells (Fig. 2G). This result might indicate that the reduction in retinal endothelial cell proliferation, filopodia formation and neovascularization is due to the lack of retinal Pak1.

p38MAPKβ regulates tip cell formation and retinal neovascularization

In order to understand the mechanisms by which Pak1 mediates retinal neovascularization, we assessed the effect of hypoxia on Pak1 phosphorylation in the retinas of WT and Pak1$^{-/-}$ mice. We observed a threefold increase in Pak1 phosphorylation at 12 h of hypoxia as compared to normoxia in WT mice retinas (Fig. 3A). As expected, the presence of Pak1 was not detected in the retinas of Pak1$^{-/-}$ mice. Pak1 mediates most of its functions by phosphorylating its downstream effector molecules such as mitogen-activated protein kinases (MAPKs) and cofilin (Arias-Romero and Chernoff, 2008; Bokoch, 2003; Dummler et al., 2009). Therefore, we next analyzed the effect of hypoxia on phosphorylation of ERK1 and ERK2 (ERK1/2, also known as MAPK3 and MAPK1, respectively), JNK1 and JNK3 (also known as MAPK8 and MAPK10, respectively) and p38MAPK family proteins in the retinas of WT and Pak1$^{-/-}$ mice in order to test the role of MAPKs in Pak1-mediated retinal neovascularization. We observed that hypoxia, although having little or no effect on ERK1/2 phosphorylation, induced JNK1 and JNK3, and p38MAPK phosphorylation (with the induction of p38MAPK being stronger), in the retinas of WT mice as compared to the retinas of Pak1$^{-/-}$ mice (Fig. 3B). Because p38MAPK phosphorylation was induced more dramatically in the retinas of WT mice and this effect was completely negated in the retinas of Pak1$^{-/-}$ mice, we next tested the role of p38MAPK on retinal neovascularization. Depletion of p38MAPKβ by its siRNA reduced retinal vasculature, neovascularization, endothelial cell proliferation and filopodia formation with significantly increased avascular area (Fig. 3C–H). These findings indicate that p38MAPKβ acts downstream of Pak1 in mediating retinal neovascularization in a mouse model of OIR.

p38MAPKβ mediates VEGFA-induced angiogenic events in HRMVECs

To explore the interrelationship between Pak1 and p38MAPKβ in VEGFA-induced angiogenic events in HRMVECs, we examined the effect of VEGFA on p38MAPK phosphorylation in HRMVECs. A time-dependent increase was observed in p38MAPK phosphorylation upon VEGFA stimulation in HRMVECs with a maximum effect at 10 min (Fig. 4A). Next, we investigated the role of Pak1 on VEGFA-induced p38MAPK phosphorylation. We inhibited Pak1 by use of dnPak1 activation or siRNA-mediated Pak1 depletion, and this had no effect on VEGFA-induced p38MAPK phosphorylation (Fig. 4B,C). By contrast, adenoviral-mediated expression of a dominant-negative (dn)p38MAPKβ

Journal of Cell Science (2016) 129, 1234-1249 doi:10.1242/jcs.179382

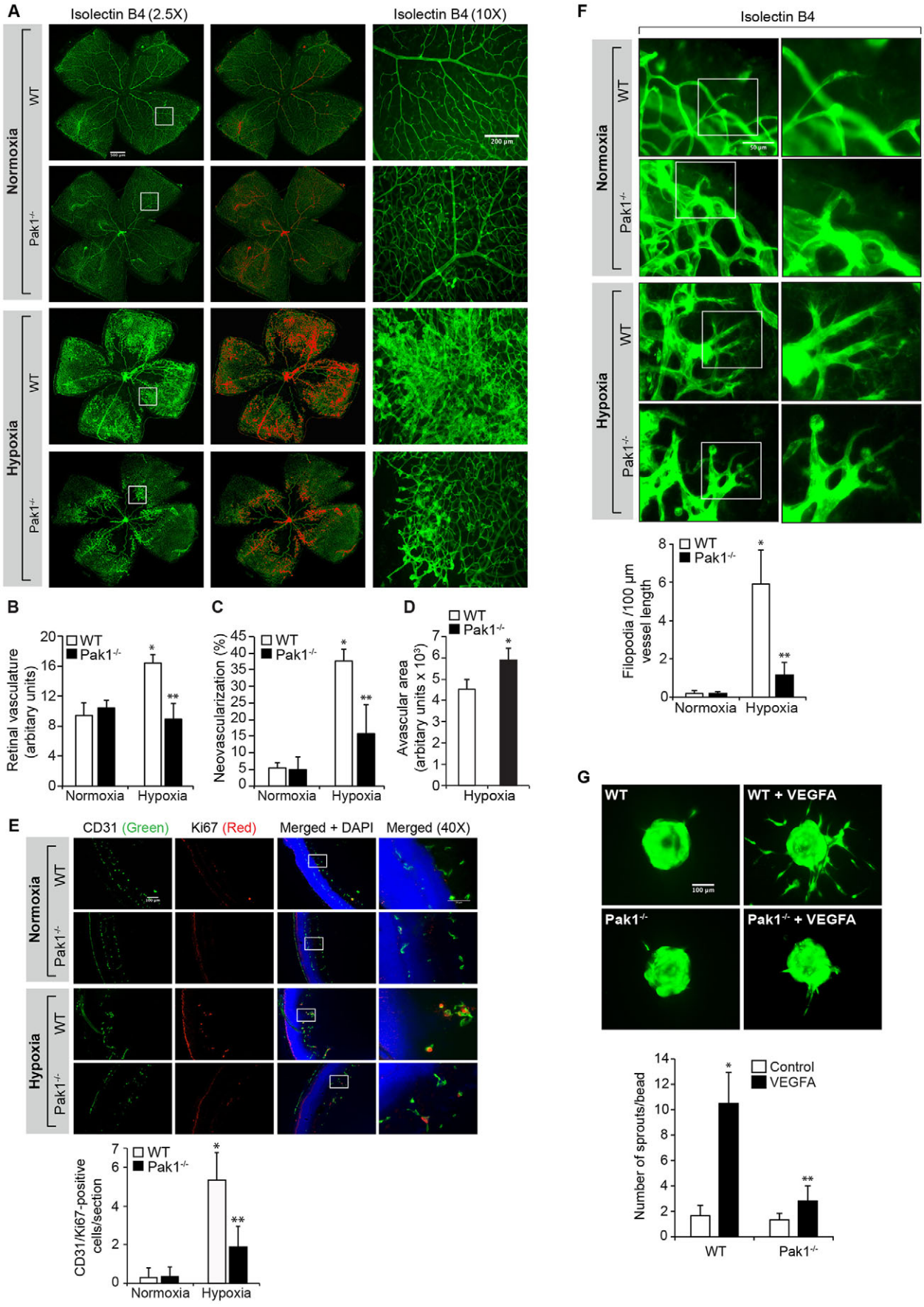

Fig. 2. See next page for legend.

Journal of Cell Science

Fig. 2. Deletion of Pak1 attenuates hypoxia-induced retinal neovascularization. (A) WT and Pak1$^{-/-}$ mice pups after exposure to 75% oxygen from P7 to P12 were returned to normal air to develop relative hypoxia. At P17, the retinas were isolated, stained with isolectin B4, and flat mounts were prepared and examined under a fluorescent microscope. Retinal vascularization is shown in the first column. Neovascularization is highlighted in red in the second column. The third column shows the selected rectangular areas of the images in the first column as viewed under 10× magnification. Scale bars: 500 µm (left two columns), 200 µm (right column). (B–D) Retinal vasculature (B), neovascularization (C) and avascular area (D) were determined as described in the Materials and Methods. (E) All the conditions were same as in A except that at P15 the retinas were isolated, fixed, and cross-sections were made and stained for immunofluorescence analysis of CD31 and Ki67. The right column shows the higher magnification (as viewed at 40× magnification) of the areas selected by the rectangular boxes in the left column images. (F) All the conditions were the same as in A except that at P15 the retinas were isolated, stained with isolectin B4, and flat mounts were made and examined for filopodia under fluorescent microscope at 40× magnification. (G) Retinal endothelial cells from WT and Pak1$^{-/-}$ mice were isolated and tested for VEGFA (40 ng/ml)-induced sprouting. The bar graphs represent quantitative analysis of three independent experiments or six retinas. The values represent mean±s.d. *P<0.01 vs WT normoxia; **P<0.01 vs WT hypoxia (one-way ANOVA followed by Tukey's post-hoc test).

mutant not only blocked VEGFA-induced Pak1 phosphorylation but also reduced its steady-state levels in HRMVECs (Fig. 4D). To further verify the specificity of the role of p38MAPKβ on Pak1 phosphorylation and its levels, we reprobed the blots for JNK1 and JNK3 phosphorylation and found that inhibition of p38MAPKβ had no effect on VEGFA-induced JNK1 and JNK3 phosphorylation or its steady-state levels (Fig. 4D). Hence, given that p38MAPKβ acts downstream of Pak1 in the mediation of retinal neovascularization in a mouse model of OIR and upstream of Pak1 in VEGFA-induced angiogenic events in HRMVECs, we next tested the role of Pak1 in p38MAPKβ activation in mouse retinal microvascular endothelial cells (MRMVECs) to validate these effects. VEGFA induced p38MAPK activation in MRMVECs, and this effect was suppressed by interference of Pak1 activation by use of its dominant-negative mutant (Fig. 4E). These findings confirm the species differences in the positional interdependence in the activation between Pak1 and p38MAPKβ in response to VEGFA. Blocking of p38MAPKβ activation by use of its dominant-negative mutant inhibited VEGFA-induced HRMVEC F-actin stress fiber formation, migration, proliferation, sprouting and tube formation (Fig. 5A–E). To confirm the positional interdependency between p38MAPKβ and Pak1 activation in HRMVECs in response to VEGFA, we also performed the rescue experiments. Overexpression of dnp38MAPKβ inhibited VEGFA-induced HRMVEC sprouting and this effect was rescued by forced expression of constitutively active Pak1 (Fig. 5F).

Role of cofilin in retinal neovascularization

Under the influence of angiogenic factors like VEGFA, endothelial cells acquire the ability to migrate and proliferate. It has been reported that inhibition of cofilin promotes actin polymerization, generates protrusions and determines the direction of cell migration (Ghosh et al., 2004). It has also been demonstrated that Pak1, through phosphorylation, inhibits cofilin activity during the regulation of cell protrusions (Delorme et al., 2007). To understand the role of cofilin in VEGFA-induced angiogenic events, we first examined the effect of VEGFA on cofilin phosphorylation in HRMVECs. Treatment of HRMVECs with VEGFA resulted in a time-dependent phosphorylation of cofilin, with a maximum effect observed at 30 min (Fig. 6A). To understand its function, cells were treated with and without VEGFA (40 ng/ml) for 30 min, and immunoprecipitated with antibodies against phosphorylated cofilin or cofilin. The immunocomplexes were then assayed for actin polymerization and severing activities. Immunoprecipitates of phosphorylated cofilin and cofilin in VEGFA-treated cells exhibited increased polymerization activity as compared to control immunoprecipitates (Fig. 6B). By contrast, only the cofilin immunocomplexes showed increased severing activity as compared to either the phosphorylated cofilin immunocomplexes of control, or both phosphorylated cofilin and cofilin immunocomplexes of VEGFA-treated cells (Fig. 6B). These results indicate that cofilin phosphorylation promotes actin polymerization in response to VEGFA. Next, we tested the role of p38MAPKβ and Pak1 on VEGFA-induced cofilin phosphorylation. Dominant-negative mutants of p38MAPKβ and Pak1 significantly blocked VEGFA-induced cofilin phosphorylation, suggesting that the p38MAPKβ–Pak1 signaling axis controls cofilin activity in HRMVECs (Fig. 6C,D). DnJNK1 had no effect on VEGFA-induced cofilin phosphorylation in HRMVECs (Fig. 6C). In order to determine the functional significance of cofilin in VEGFA-induced angiogenic responses of HRMVECs, we tested the effect of its phosphorylation mutant, cofilin S3A. Transfection of cells with cofilin S3A plasmid inhibited VEGFA-induced cofilin phosphorylation, F-actin stress fiber formation, migration, DNA synthesis, sprouting and tube formation (Fig. 6E–J). Similarly, downregulation of cofilin by use of its siRNA also attenuated VEGFA-induced HRMVEC F-actin stress fiber formation, migration, DNA synthesis, sprouting and tube formation (Fig. 7A–F). These findings infer that recycling of G-actin is needed for VEGFA-induced HRMVEC F-actin stress fiber formation, and thereby in the migration, DNA synthesis, sprouting and tube formation of these cells. To further show that the Pak1-mediated HRMVEC angiogenic responses are mostly dependent on its downstream effector cofilin, and not due to its nonspecific effects, we also tested a role for Pak1 in activation of p70S6K (also known as RPS6KB1). VEGFA induced p70S6K activation very strongly, and inhibition of Pak1 by use of its dominant-negative mutant or downregulaton of its steady state levels by use of its siRNA had no effect on VEGFA-induced p70S6K activation. These findings infer that Pak1 effects on VEGFA-induced HRMVEC angiogenic responses are selective (Fig. 7G).

To understand the role of cofilin in tip cell formation and retinal neovascularization, we first studied the effect of hypoxia on cofilin phosphorylation. Hypoxia induced the phosphorylation of cofilin in retina with a fivefold increase at 24 h (Fig. 8A). Genetic deletion of Pak1 or siRNA-mediated downregulation of p38MAPKβ attenuated the effect of hypoxia on cofilin phosphorylation (Fig. 8A,B). No change in cofilin phosphorylation was observed in JNK1-depleted retinas (Fig. 8B). Because cofilin inactivation promotes actin polymerization and cell migration (Ghosh et al., 2004), we next tested the effect of cofilin depletion on hypoxia-induced retinal vasculature, neovascularization, endothelial cell proliferation and tip cell formation. Depletion of cofilin levels by using its siRNA led to a reduction in retinal vasculature, neovascularization (as observed by decreased tufts) and tip cell formation (Fig. 8C–E,G). We also observed an increase in the avascular area in cofilin-depleted hypoxic retinas (Fig. 8F). Furthermore, depletion of cofilin levels significantly reduced retinal endothelial cell proliferation as compared to control siRNA (Fig. 8H).

DISCUSSION

Ischemia-induced pathological retinal neovascularization is a common manifestation of various retinal disorders, including retinopathy of prematurity and diabetic retinopathy (Aiello, 2005; Mechoulam and Pierce, 2003). In both the conditions, the hypoxic

Journal of Cell Science (2016) 129, 1234-1249 doi:10.1242/jcs.179382

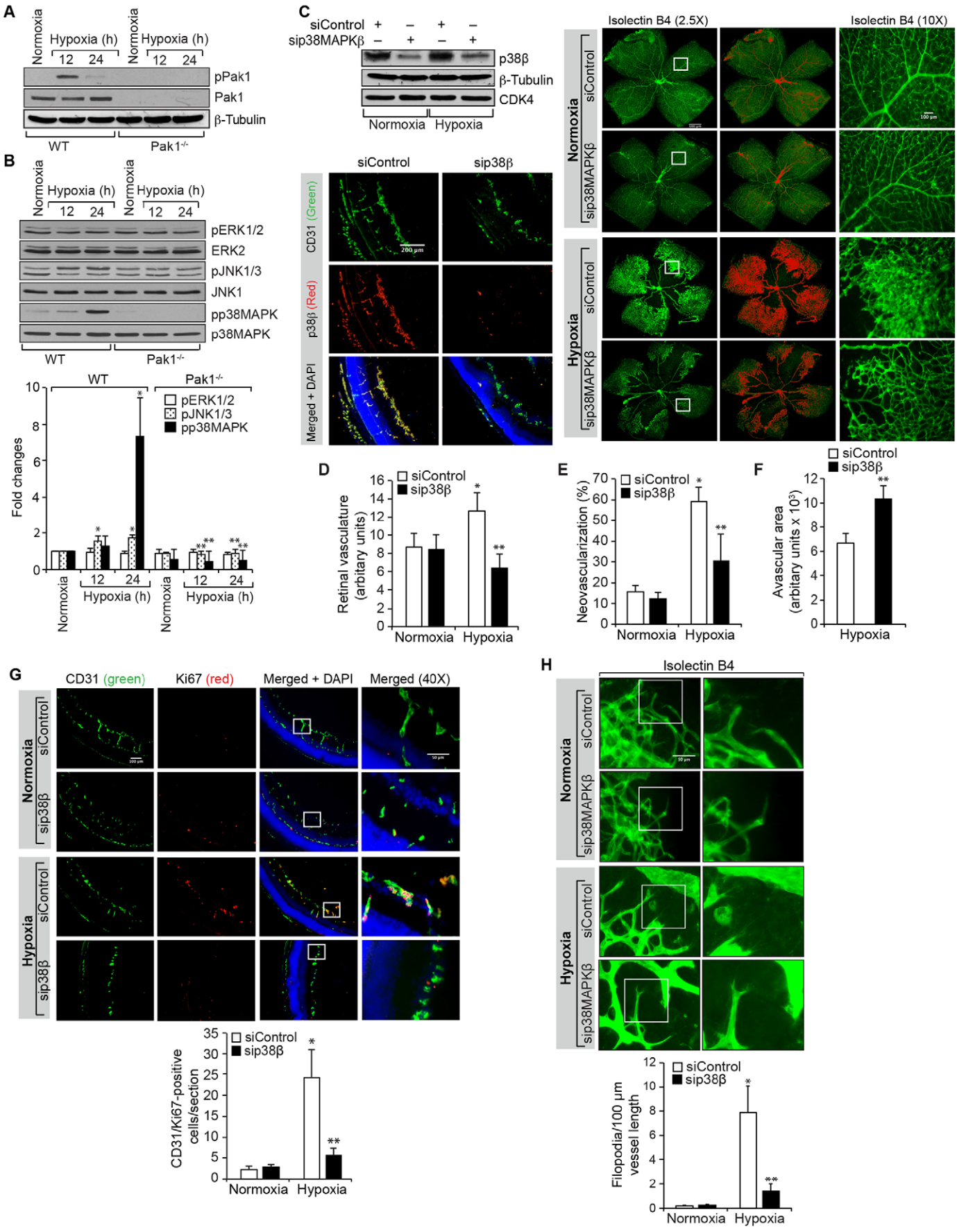

Fig. 3. See next page for legend.

Journal of Cell Science (2016) 129, 1234-1249 doi:10.1242/jcs.179382

Fig. 3. p38MAPKβ mediates hypoxia-induced retinal neovascularization. (A,B) Eyes from WT and Pak1$^{-/-}$ mice pups left in normoxia or at various time periods of hypoxia were enucleated, retinas were isolated and extracts were prepared. An equal amount of protein from each condition was analyzed by western blotting for the indicated phosphoproteins using their phosphospecific antibodies and normalized to their total levels. p, phosphorylated form of the protein. (C) WT mice pups after exposure to 75% oxygen from P7 to P12 were injected intravitreally with control siRNA (siControl) or p38MAPKβ siRNA (sip38MAPKβ) at P12, P13 and P15. At P15 the retinas were isolated and tissue extracts were prepared and analyzed by western blotting for p38MAPKβ (p38β), β-tubulin and CDK4 levels to show the efficacy of the siRNA on its target and off target molecules. Alternatively, retinas were fixed, and cut sections were stained for CD31 and p38MAPKβ to show the effect of the siRNA on its target molecule level in endothelial cells, or at P17 the retinas were isolated, stained with isolectin B4, and flat mounts were prepared and examined for retinal neovascularization. Retinal vascularization is shown in the first column. Neovascularization is highlighted in red in the second column. The third column shows the selected rectangular areas of the images in the first column under 10× magnification. Scale bars: 500 µm (right panel, left two columns), 200 µm (right panel, right column). (D–F) Retinal vasculature (D), neovascularization (E) and avascular area (F) were determined as described in the Materials and Methods. (G) All the conditions were the same as in C except that mice pups were injected intravitreally with control or p38MAPKβ siRNA at P12 and P13 and at P15, the retinas were isolated, fixed, and cross-sections were made and stained for immunofluorescence analysis of CD31 and Ki67. The right column shows the areas selected by the rectangular boxes in the left column images as viewed under higher magnification (40×). (H) All the conditions were the same as in G except that at P15 the retinas were isolated, stained with isolectin B4, and flat mounts were made and examined for filopodia under the fluorescent microscope at 40× magnification. The bar graphs represent quantitative analysis of three independent experiments or six retinas. The values represent mean±s.d. *P<0.01 vs WT normoxia; **P<0.01 vs WT hypoxia (one-way ANOVA followed by Tukey's post-hoc test).

retina increases the expression of proangiogenic factors that stimulate retinal endothelial cell sprouting and neovascularization (Arden and Sivaprasad, 2011; Hellström et al., 2013; Smith et al., 2013). Sprouting angiogenesis is a process in which new vascular loops are formed from the existing ones to expand the vasculature (Potente et al., 2011). VEGFA promotes endothelial cell migration, proliferation and sprouting both *in vitro* and *in vivo* (Gerber et al., 1998; Hellström et al., 2007). In recent years various signaling pathways have been studied in order to understand the process of angiogenic sprouting (Adams and Alitalo, 2007; Jakobsson et al., 2010). However, the mechanisms by which endothelial cells migrate and form sprouts are not well understood. In the present study, we provide evidence that Pak1–p38MAPKβ-dependent cofilin phosphorylation and inhibition is involved in hypoxia-induced endothelial tip cell formation and retinal neovascularization. In contrast, our *in vitro* studies using HRMVECs show that p38MAPKβ acts upstream of Pak1 in cofilin phosphorylation and inhibition in mediating VEGFA-induced angiogenic events. Thus, these findings demonstrate a role for Pak1-dependent cofilin inhibition in sprouting angiogenesis and pathological retinal neovascularization with p38MAPKβ acting either upstream or downstream to Pak1, depending on the species of investigation. Furthermore, the role of the Pak1–cofilin signaling axis in VEGFA-induced HRMVEC angiogenic events is specific, as interference with activation of Pak1 does not affect other signaling events such as p70S6K activation by VEGFA.

The early stages of endothelial tip cell formation and sprouting involve extensive cytoskeleton remodeling and disruption of cell adhesions, in which Pak1 plays an essential role (Bokoch, 2003). Along with these events, Pak1 regulates the development and function of various organ systems, such as heart and blood vessels (Ke et al., 2004; Liu et al., 2007; Radu et al., 2014). Although many studies have shown a role for signaling molecules that act either upstream or downstream of Pak1 in angiogenesis and vasculogenesis (Hu et al., 2011; Srinivasan et al., 2009; Tan et al., 2008), there are no reports that provide direct evidence for the role of Pak1 in these processes. In this context, in the present study, we demonstrate that inhibition of Pak1 by use of its dominant negative mutant reduces the amount of VEGFA-induced F-actin stress fiber formation, migration, proliferation, sprouting and tubulogenesis in HRMVECs. In addition, using a mouse model of OIR, we observed a reduction in hypoxia-induced endothelial cell proliferation, tip cell formation and neovascularization in Pak1$^{-/-}$ mice retinas as compared to WT mice retinas. These findings provide a direct evidence for the role of Pak1 in pathological retinal angiogenesis.

Previously, it has been reported that VEGF and FGF2 induce Pak1 activation (Hood et al., 2003). Furthermore, Pak1 phosphorylates and activates MEK1 (Slack-Davis et al., 2003), ERK1/2 (Beeser et al., 2005) and p38MAPK (Dechert et al., 2001). Towards identifying the downstream signaling molecules in Pak1-mediated retinal neovascularization, here we demonstrate that hypoxia induces p38MAPK phosphorylation in the mouse retina in a Pak1-dependent manner and p38MAPKβ downregulation, by use of its siRNA, results in reduced retinal endothelial cell proliferation, tip cell formation and neovascularization. These results are in line with the published findings on the role of p38MAPK in pathological angiogenesis (Rajashekhar et al., 2011). However, it is interesting to note that, in HRMVECs, p38MAPKβ appears to act upstream of Pak1 in mediating VEGFA-induced angiogenic events, as interference with activation of Pak1 or depletion of its levels did not affect p38MAPKβ phosphorylation but rather blockade of p38MAPKβ activation resulted in the attenuation of VEGFA-induced Pak1 phosphorylation. Furthermore, constitutively active Pak1 rescued VEGFA-induced HRMVEC sprouting from inhibition by dnp38MAPKβ. In contrast, suppression of p38MAPK activation was observed in Pak1$^{-/-}$ mouse retina in response to hypoxia and in Pak1$^{-/-}$ mouse retinal endothelial cells in response to VEGFA, indicating that in mouse endothelial cells Pak1 acts upstream to p38MAPK. These differences in the positional interdependence between Pak1 and p38MAPKβ activation in HRMVECs versus MRMVECs reflect species differences in VEGFA-induced angiogenic signaling events. The reduction in the expression levels of Pak1 in dnp38MAPKβ-infected HRMVECs suggests that p38MAPKβ could be involved in the modulation of the steady-state levels of Pak1 in HRMVECs and this could account for the attenuation in VEGFA-induced phosphorylation and activation of Pak1 upon prevention of p38MAPKβ activation.

Many studies show that cofilin inhibition downstream of Pak1 is required for actin polymerization in generating lamellipodia and filopodia and determining the direction of cell migration (Ghosh et al., 2004; Delorme et al., 2007). Here, we found that cofilin phosphorylation and inhibition downstream of p38MAPKβ-Pak1 signaling mediates VEGFA-induced F-actin stress fiber formation, migration, proliferation, sprouting and tubulogenesis in HRMVECs. Our results also demonstrate that cofilin plays a role in hypoxia-induced tip cell formation and retinal neovascularization, as downregulation of cofilin levels reduced these effects. Given that downregulation of cofilin levels reduced HRMVEC F-actin stress fiber formation, migration, proliferation, sprouting and tube formation *in vitro*, and hypoxia-induced endothelial cell proliferation, tip cell formation and neovascularization *in vivo*, it is likely that inactivation and activation cycles of cofilin are essential for its role in actin cytoskeleton remodeling. Indeed, either inhibition of cofilin by its phosphorylation or depletion of its

Journal of Cell Science (2016) 129, 1234-1249 doi:10.1242/jcs.179382

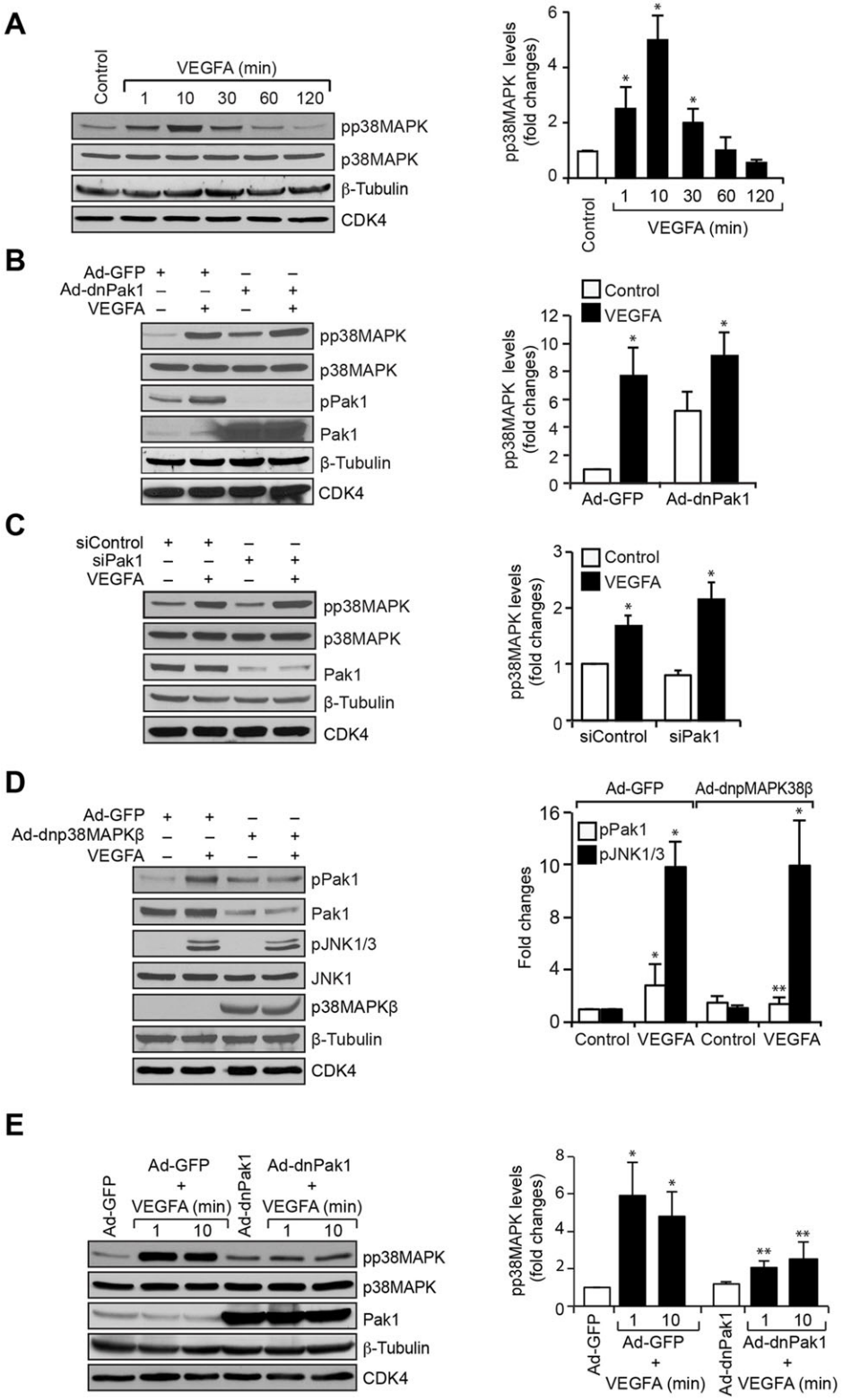

Fig. 4. p38MAPKβ mediates Pak1 activation. (A) Quiescent HRMVECs were treated with and without VEGFA (40 ng/ml) for the indicated time periods and cell extracts were prepared. Equal amounts of protein from control and each treatment were analyzed by western blotting for phosphorylated (p)p38MAPK using its phosphospecific antibodies and normalized to its total levels, as well as to β-tubulin and CDK4 levels. (B) Cells were transduced with Ad-GFP or Ad-dnPak1 at 40 MOI, growth-arrested, and treated with and without VEGFA (40 ng/ml) for 10 min. Then, cell extracts were prepared and analyzed by western blotting for pp38MAPK and phosphorylated (p)Pak1 levels using their phosphospecific antibodies and reprobed for p38MAPK, Pak1, β-tubulin or CDK4 levels for normalization or to show the overexpression of dnPak1. (C) HRMVECs were transfected with control or Pak1 siRNA (100 nM), growth-arrested, treated with and without VEGFA (40 ng/ml) for 10 min. Then, cell extracts were prepared and an equal amount of protein from control and each treatment was analyzed by western blotting for pp38MAPK levels using its phosphospecific antibodies and reprobed for p38MAPK, Pak1, β-tubulin or CDK4 levels to show the efficacy of the siRNA on its target and off target molecules. (D) Cells were transduced with Ad-GFP or Ad-dnp38MAPKβ at 40 MOI, growth-arrested, treated with and without VEGFA (40 ng/ml) for 10 min. Then, cell extracts were prepared and analyzed by western blotting for pPak1 and phosphorylated (p)JNK1 and JNK3 levels using their phosphospecific antibodies and reprobed for Pak1, JNK1, p38MAPKβ, β-tubulin or CDK4 levels for normalization or to show the overexpression of dominant negative p38MAPKβ. (E) Mouse retinal microvascular endothelial cells were transduced with Ad-GFP or Ad-dnPak1 at 40 MOI, growth-arrested, treated with and without mouse VEGFA (40 ng/ml) for 1 and 10 min. Then, cell extracts were prepared and analyzed by western blotting for pp38MAPK levels using its phosphospecific antibodies, and reprobed for p38MAPK, Pak1, β-tubulin or CDK4 levels for normalization or to show the overexpression of dnPak1. The bar graphs represent quantitative analysis of three independent experiments. The values represent mean±s.d. *P<0.01 vs control, Ad-GFP or siControl; **P<0.01 vs VEGFA, Ad-GFP+VEGFA or siControl+ VEGFA (one-way ANOVA followed by Tukey's post-hoc test).

levels leads to defective lamellipodia formation and migration (Hotulainen et al., 2005; Kiuchi et al., 2007). Although a large body of evidence suggests that there is a role for cofilin in F-actin stress fiber formation and cell migration, very little is known about its role in cell proliferation. In this context, the present findings show that downregulation of cofilin reduces endothelial cell proliferation, a finding that demonstrates the role of cofilin in the regulation of cell proliferation. One possible mechanism by which cofilin might be involved in the regulation of cell proliferation could be through influencing the cellular location of some signaling molecules that play a role in cell proliferation. For example, a recent study has shown that cofilin and ERK5 (also known as MAPK7) facilitate the recruitment of PAF1 to RNA polymerase II and enhances gene expression in response to estrogen receptor α (Madak-Erdogan

Journal of Cell Science (2016) 129, 1234-1249 doi:10.1242/jcs.179382

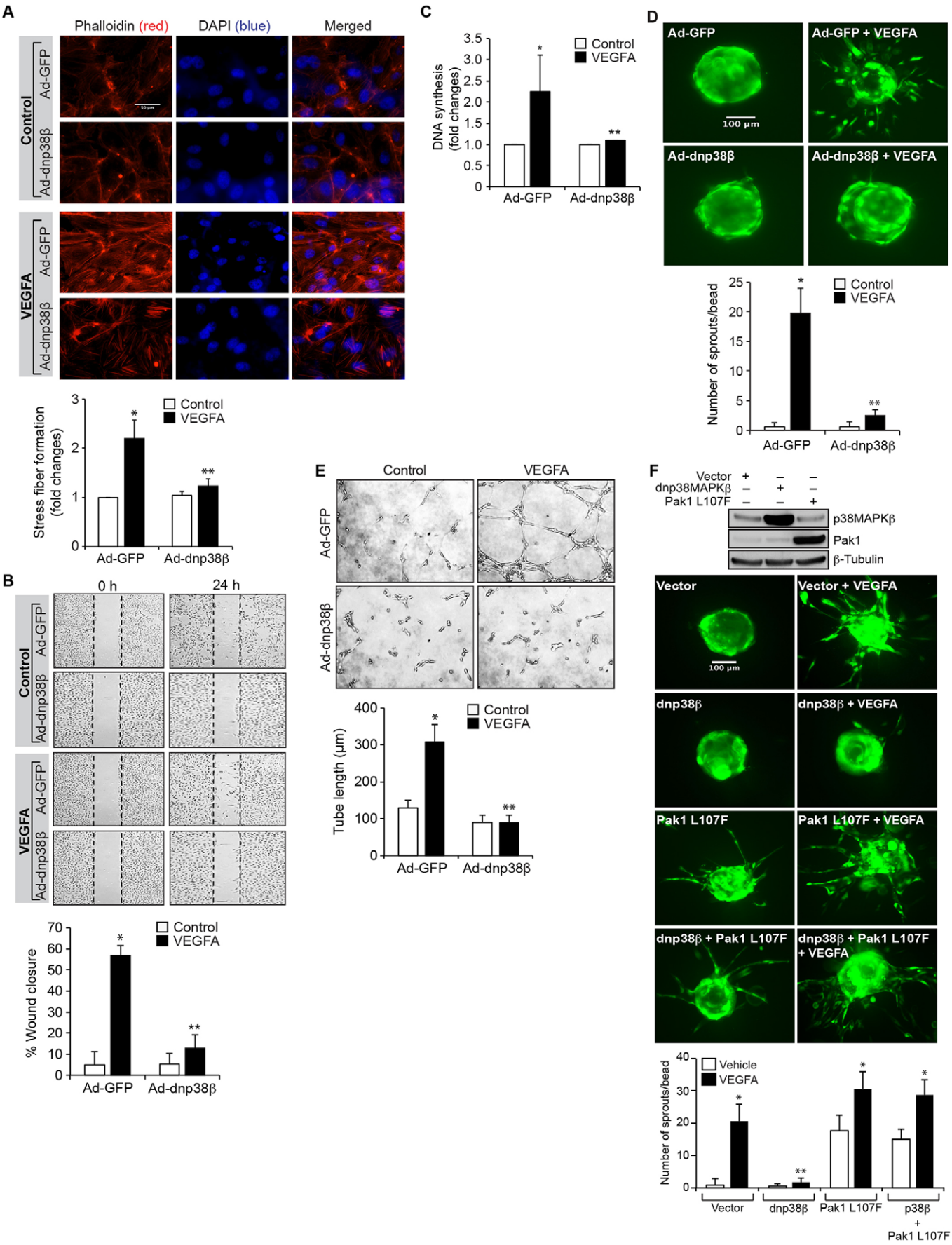

Fig. 5. See next page for legend.

Fig. 5. p38MAPKβ mediates VEGFA-induced HRMVEC angiogenic events. (A) HRMVECs were transduced with Ad-GFP or Ad-dnp38MAPKβ at 40 MOI, growth-arrested, treated with and without VEGFA (40 ng/ml) for 2 h and stained with phalloidin to assess F-actin stress fiber formation. The changes in stress fiber levels were assessed by measuring the fluorescence intensity, and are presented as the fold changes relative to control. Scale bars: 50 µm. (B–E) All the conditions were the same as in A, except that cells were treated with and without VEGFA (40 ng/ml) and subjected to migration (B), DNA synthesis (C), sprouting (D) or tube formation (E) assays. (F) Upper panel, cells were transfected with vector, dnp38MAPKβ or Pak1 L107F plasmid (1.5 µg/ml). Then, cell extracts were prepared and an equal amount of protein from each condition was analyzed by western blotting for p38MAPKβ or Pak1 levels using their specific antibodies to show their overexpression, and the blot was reprobed for β-tubulin levels for normalization. Lower panel, all the conditions were the same as in the upper panel except that cells were subjected to an VEGFA (40 ng/ml)-induced sprouting assay. The bar graphs represent quantitative analysis of three independent experiments. The values represent mean±s.d. **P*<0.01 vs Ad-GFP; ***P*<0.01 vs Ad-GFP+VEGFA (one-way ANOVA followed by Tukey's post-hoc test).

et al., 2014). In summary, the present findings demonstrate that Pak1–p38MAPKβ–cofilin signaling, by influencing cytoskeleton remodeling, enhances endothelial cell migration, proliferation, tip cell formation and sprouting leading to retinal neovascularization.

MATERIALS AND METHODS

Reagents

Growth-factor-reduced Matrigel (354230) was obtained from BD Biosciences (Bedford, MA). Recombinant human VEGF165 (293-VE-010/CF) and recombinant mouse VEGF164 (493-MV-005/CF) were bought from R&D Systems (Minneapolis, MN). Anti-phosphorylated-cofilin (for immunoprecipitation, 1:25, SC-12912R), anti-ERK2 (for immunoblotting, 1:500, SC-154), anti-GFP (for immunoblotting, 1:500, SC-9996) and anti-β-tubulin (for immunoblotting, 1:1000, SC-9104) antibodies and normal rabbit IgG (for immunoprecipitation, 1:25, SC-2027) were purchased from Santa Cruz Biotechnology (Santa Cruz, CA). Anti-cofilin (for immunoblotting, 1:1000, 5175), anti-phosphorylated-cofilin (for immunoblotting, 1:1000, 3311), anti-phosphorylated-ERK1/2 (for immunoblotting, 1:1000, 9101), anti-phosphorylated-p38MAPK (for immunoblotting, 1:1000, 9215), anti-Pak1 (for immunoprecipitation, 1:250; for immunoblotting, 1:1000, 2602), anti-Pak2 (for immunoprecipitation, 1:250; for immunoblotting, 1:1000, 2608) and anti-Pak3 (for immunoprecipitaion, 1:250; for immunoblotting, 1:1000, 2609) antibodies were obtained from Cell Signaling Technology (Beverly, MA). Anti-CD31 (for immunofluorescence, 1:100, 550274) antibody was purchased from BD Pharmingen (Palo Alto, CA). Anti-Cofilin (for immunoprecipitation, 1:250, ab11062), anti-phosphorylated-Pak1 (for immunoblotting, 1:1000, ab2477) and anti-Ki67 (for immunofluorescence, 1:100, ab15580) antibodies were obtained from Abcam (Cambridge, MA). Control non-targeting small interfering RNA (siRNA) (D-001810-10), mouse p38MAPKβ siRNA (ON-TARGET plus SMARTpool L-050928-00-0010), mouse cofilin1 siRNA (ON-TARGET plus SMARTpool L-058638-01-0010) and human cofilin1 siRNA (ON-TARGET plus SMARTpool L-012707-00-0010) were obtained from Dharmacon (Pittsburgh, PA). Rhodamine–phalloidin (00027) was obtained from Biotium, Inc. (Hayward, CA). Alexa-Fluor-488-conjugated goat anti-rat-IgG, Alexa-Fluor-568-conjugated goat anti-rabbit-IgG, Hoechst 33342, isolectin B4-594, and Prolong Gold antifade reagent were bought from Molecular Probes (Eugene, OR). [^{3}H]Thymidine (specific activity of 20 Ci/mM) was obtained from Perkin Elmer (Boston, MA). pEGFP-N1 human cofilin (WT) and cofilin S3A (mutant) were gifts from James Bamburg (Addgene plasmid 50859 and 50860, respectively) (Garvalov et al., 2007). pCMV6M-Pak1 L107F (CA-Pak1) was a gift from Jonathan Chernoff (Addgene plasmid # 12212) (Xiao et al., 2002).

Animals

Pak1$^{-/-}$ mice on C57BL/6 background were obtained from Mutant Mouse Regional Resource Center, University of North Carolina at Chapel Hill, Chapel Hill, NC and bred at the University of Tennessee HSC vivarium. The F2 generation pups were used in the study. All the experiments involving mice were approved by the Animal Care and Use Committee of the University of Tennessee Health Science Center, Memphis, TN.

Cell culture

Human retinal microvascular endothelial cells (HRMVECs) (ACBRI 181) were purchased from Applied Cell Biology Research Institute (Kirkland, WA) and cultured in medium 131 containing microvascular growth supplements (MVGS), 10 µg/ml gentamycin, and 0.25 µg/ml amphotericin B. Cultures were maintained at 37°C in a humidified 95% air and 5% CO_2 atmosphere. HRMVECs with passage numbers between 5 and 10 were synchronized by incubating in medium 131 without MVGS for 24 h and used to perform the experiments unless otherwise indicated.

Isolation of mouse retinal microvascular endothelial cells

Eyes from 3-week-old WT and Pak1$^{-/-}$ mice pups were enucleated, retinas dissected out, minced and digested in 4 ml of collagenase type I [1 mg/ml in serum-free Dulbecco's modified Eagle's medium (DMEM); LS004196, Worthington, Lakewood, NJ] for 60 min at 37°C. Following digestion, an equal volume of DMEM containing 10% fetal bovine serum (FBS) was added and the cellular digest was filtered through a sterile 40-µm nylon mesh (352340, BD Biosciences, San Jose, CA) and centrifuged at 250 ***g*** for 5 min to pellet the cells. The cell pellet was washed twice with DMEM containing 10% FBS, resuspended in 1.0 ml of DMEM with 10% FBS and incubated with sheep anti-rat-IgG magnetic beads pre-coated with rat anti-mouse-CD31 antibodies [sheep anti-rat Dynabeads (11035, Life Technologies, Grand Island, NY) were washed three times with serum-free DMEM and incubated with rat anti-mouse-CD31 antibody (550330, BD Biosciences, San Jose, CA) overnight at 4°C (10 µl antibody/50 µl beads in DMEM)]. After affinity binding, magnetic beads were washed six times with DMEM containing 10% FBS and the bound cells were plated onto a single well of a 24-well plate. Mouse retinal endothelial cells were cultured in EGM-2 medium containing 20% FBS at 37°C in humidified 95% air and 5% CO_2 and synchronized in EBM-2 medium without any growth supplements for 24 h to perform the experiments.

Adenoviral vectors

The construction of Ad-GFP, Ad-dnPak1, Ad-dnp38β was described previously (Dechert et al., 2001; Hedges et al., 1999; Liu et al., 2005; Sells et al., 1997).

Actin polymerization and severing assay

The actin polymerization and severing activity was measured by using the pyrene-actin polymerization kit (BK003, Cytoskeleton, Inc.) following the manufacturer's instructions. Briefly, cell extracts of control and VEGFA-treated cells were immunoprecipitated with anti-cofilin or anti-phosphorylated-cofilin antibodies. The cofilin was eluted from the beads with 0.2 M glycine (pH 2.6) and neutralized by the addition of an equal volume of 20 mM Tris-HCl (pH 8.5). To measure actin-polymerization activity, stock pyrene-actin was diluted to 2.3 µM with actin buffer (5 mM Tris-HCl, pH 8.0 and 0.2 mM $CaCl_2$) containing 0.2 mM ATP and 0.5 mM DTT and stored on ice for 60 min to depolymerize the actin oligomers. The actin monomers were collected by centrifugation at 18,800 ***g*** for 30 min at 4°C. The pyrene-actin monomers were mixed with the eluted cofilin or phosphorylated cofilin in a 96-well plate containing polymerization buffer (25 mM KCl and 1 mM $MgCl_2$, pH 7.0). The kinetics of actin polymerization was measured by assessing the fluorescence intensity generated by pyrene release for 1 h in a SpectraMax Gemini XS spectrofluorometer (Molecular Devices) at 355 nm excitation and 405 nm emission. For severing activity, F-actin was prepared by incubating pyrene-actin (30 mg/ml) in a polymerization buffer (50 mM KCl, 2 mM $MgCl_2$, 0.5 mM ATP, 2 mM Tris-HCl, pH 8.0) for 1 h at room temperature. The eluted cofilin or phosphorylated cofilin from the immunocomplexes was incubated with F-actin in a 96-well plate and the rate of the loss of fluorescence intensity was measured at 530 excitation and 590 nm emission.

Cell migration

HRMVEC migration was measured by a wound-healing assay. Briefly, HRMVECs were plated at 2×10^5 cells/ml in each chamber of the ibidi culture inserts, grown to full confluency so that growth was arrested.

Journal of Cell Science (2016) 129, 1234-1249 doi:10.1242/jcs.179382

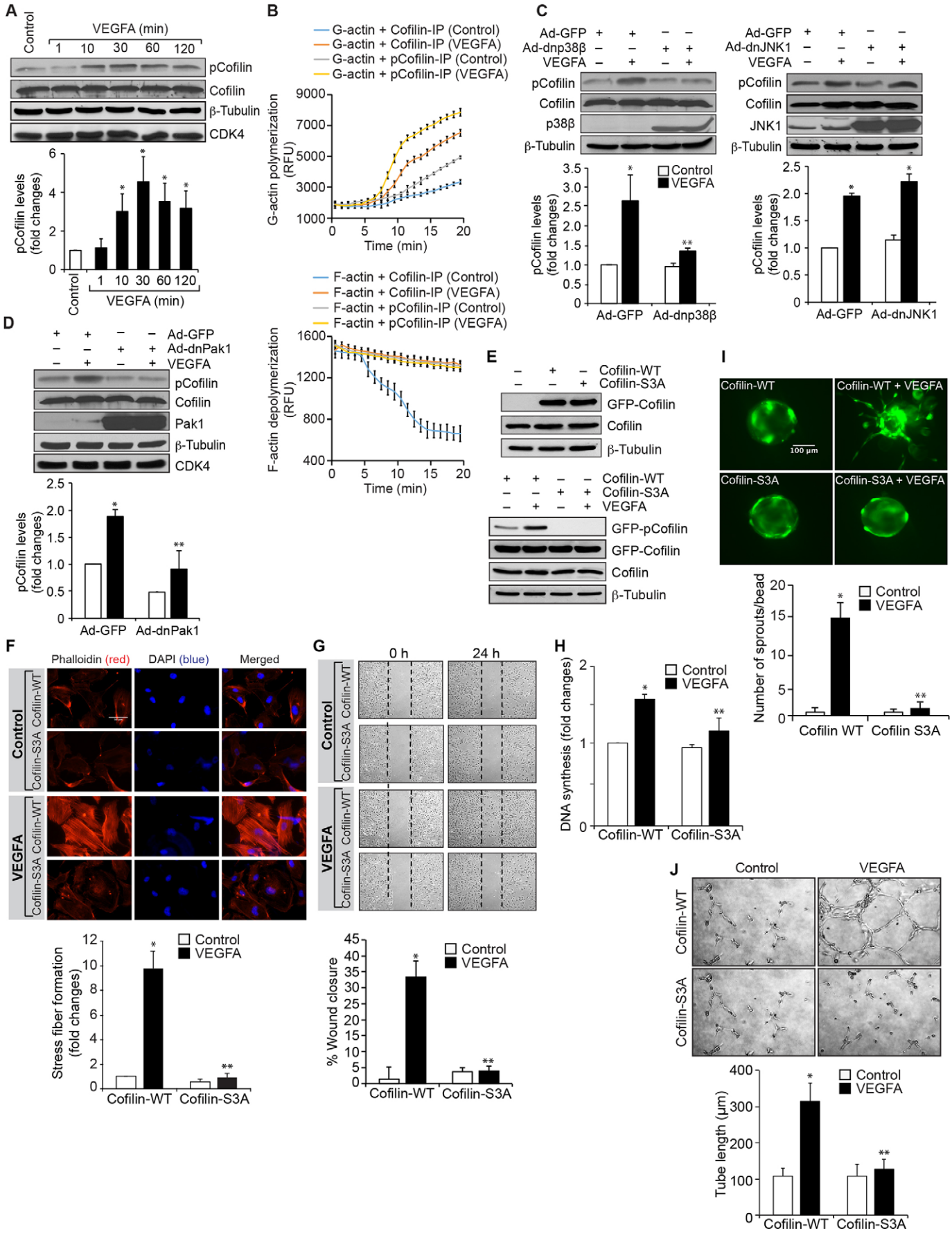

Fig. 6. See next page for legend.

Fig. 6. Cofilin regulates VEGFA-induced angiogenic events in HRMVECs. (A) Quiescent HRMVECs were treated with and without VEGFA (40 ng/ml) for the indicated time periods and cell extracts were prepared. Equal amounts of protein from control and each treatment were analyzed by western blotting for phosphorylated (p)cofilin levels using its phosphospecific antibody. (B) Antibody-immunoprecipitated (IP) cofilin and phosphorylated cofilin immunocomplexes of control and 30 min of VEGFA (40 ng/ml)-treated cells were subjected to an assay to measure their actin polymerization and severing activities as described in the Materials and Methods. (C,D) HRMVECs were transduced with Ad-GFP, Ad-dnp38MAPKβ, Ad-dnJNK1 or Ad-dnPak1 at 40 MOI, growth-arrested, treated with and without VEGFA (40 ng/ml) for 30 min. Then, cell extracts were prepared and analyzed by western blotting for phosphorylated cofilin levels as described in panel A. The blots in panels A,C and D were reprobed for cofilin, p38MAPKβ, JNK1, Pak1, β-tubulin or CDK4 for normalization or to show the overexpression of the indicated dominant-negative mutants. (E) Upper panel, HRMVECs were transfected with GFP-tagged cofilin WT or cofilin S3A mutant plasmid and, 36 h later, cell extracts were prepared and analyzed by western blotting for cofilin levels to show the overexpression of WT and phosphomutant cofilin. Lower panel, after transfection, cells were growth-arrested, treated with and without VEGFA (40 ng/ml) for 30 min and cell extracts were prepared and analyzed by western blotting for phosphorylated and normal coflin levels and the blots were normalized to β-tubulin. (F–J) All the conditions were the same as in bottom panel of E except that after quiescent cells were subjected to VEGFA (40 ng/ml)-induced F-actin stress fiber formation (F, scale bars: 50 µm), migration (G), DNA synthesis (H), sprouting (I) or tube formation (J) assays. The bar graphs represent a quantitative analysis of three independent experiments. The values represent mean±s.d. *P<0.01 vs Ad-GFP or cofilin WT; **P<0.01 vs Ad-GFP+VEGFA or cofilin WT+VEGFA (one-way ANOVA followed by Tukey's post-hoc test).

Following a 24-h growth arrest period, the inserts were removed using sterile tweezers and 1 ml of medium 131 containing 5 mM hydroxyurea was added. Cells were treated with and without VEGFA (40 ng/ml) for 24 h at which time period the migrated cells were observed under Nikon Eclipse TS100 microscope with a 4×0.13 NA objective and the images were captured with a Nikon Digital Sight DS-L1 camera. The cell migration was expressed as percentage wound closure (total area−area not occupied by the cells/total area×100).

DNA synthesis

DNA synthesis was measured by [^{3}H]thymidine incorporation (Singh et al., 2013). HRMVECs were plated onto 60-mm dishes, allowed to grow to 70–80% confluence, and then growth arrested for 24 h. Growth-arrested HRMVECs were exposed to VEGFA (40 ng/ml) and after 6 h the cells were added with 1 µCi/ml of [^{3}H]thymidine and incubation continued for another 24 h. After the incubation period, cells were harvested by trypsinization followed by centrifugation. The cell pellet was resuspended in cold 10% (w/v) trichloroacetic acid and vortexed vigorously to lyse cells. The cell lysis mixture was allowed to remain on ice for 30 min and was then passed through a GF/F glass microfiber filter. The filter was washed once with cold 5% trichloroacetic acid, once with cold 70% ethanol, dried, and placed in a liquid scintillation vial containing the liquid scintillation fluid. The radioactivity was measured in a liquid scintillation counter (Beckman LS 3801) and DNA synthesis was expressed as counts/min/dish.

Tube formation

Tube formation was measured as follows. Culture plates (24-well; Corning) were coated with 280 µl/well of growth-factor-reduced Matrigel (BD Biosciences) and allowed to solidify for 30 min at 37°C. HRMVECs were trypsinized, neutralized with trypsin neutralizer, and resuspended at 5×10^5 cells/ml, and 300 µl of this cell suspension was added into each well. Vehicle or VEGFA (40 ng/ml) was added to the appropriate wells and the cells were incubated at 37°C for 6 h. Wherever the effect of a dominant-negative mutant or siRNA was tested, cells were transduced or transfected with the respective adenovirus or siRNA at 40 multiplicity of infection (MOI) and 100 nM, respectively, and allowed to become quiescent before subjecting the cells to a tube formation assay. Tube formation was observed under an inverted microscope (Eclipse TS100; Nikon, Tokyo, Japan). Images were captured with a CCD color camera (KP-D20AU; Hitachi, Ibaraki, Japan) using Apple iMovie 7.1.4 software. The tube length was calculated using NIH ImageJ and expressed in micrometers.

Western blotting

Cell or tissue extracts containing an equal amount of protein were resolved by electrophoresis on 0.1% [weight/volume (w/v)] sodium dodecyl sulfate (SDS) and 10% (w/v) polyacrylamide gels. The proteins were transferred electrophoretically to a nitrocellulose membrane. After blocking in either 5% (w/v) nonfat dry milk or bovine serum albumin, the membrane was probed with the appropriate primary antibodies followed by incubation with horseradish-peroxidase-conjugated secondary antibodies. The antigen–antibody complexes were detected using an enhanced chemiluminescence detection reagent kit (Amersham Biosciences).

Transfections

HRMVECs were transfected with control or target gene siRNA molecules at a final concentration of 100 nM using Lipofectamine 2000 transfection reagent according to the manufacturer's instructions. After transfection, cells were growth-arrested in MVGS-free medium 131 for 24 h and then used as required. In the case of transfections *in vivo*, siRNA molecules at 1 µg in 0.5 µl per eye were injected intravitreally using a 33G needle.

F-actin stress fiber formation

F-actin stress fiber formation in HRMVECs was measured as described previously (Kundumani-Sridharan et al., 2013). HRMVECs were grown on glass coverslips and after appropriate treatments, cells were fixed in 3.7% formaldehyde in PBS for 20 min, permeabilized in 0.2% Triton X-100 for 5 min and blocked with 1% bovine serum albumin in PBS. Cells were then stained with 20 mM Rhodamine-labeled phalloidin (Biotium, Hayward, CA) for 30 min. Fluorescence was observed under a Zeiss inverted microscope (Zeiss Observer.Z1; with an ×10 NA 0.45 objective) and the fluorescence images were captured by a Zeiss AxioCam MRm camera using the microscope operating and image analysis software AxioVision 4.7.2 (Carl Zeiss Imaging Solutions GmbH). The fluorescence intensity of the stress fibers was quantified using Nikon NIS-Elements software version AR 3.1 and expressed as fold change over control.

Sprouting assay

Three-dimensional sprouting was performed according to the method of Nakatsu and Hughes (2008). Briefly, the transduced or transfected HRMVECs were coated on Cytodex beads and were allowed to attach overnight followed by embedding the beads in fibrin (2 mg/ml fibrinogen plus 0.625 units/ml of thrombin) gels. Then fibroblasts were plated on top of the fibrin gels. The beads were examined on day 5 for sprouting under a Zeiss inverted fluorescence microscope (Observer.Z1; with an ×10 NA 0.45 objective) and the fluorescence images were captured by a Zeiss AxioCam MRm camera using the microscope operating and image analysis software AxioVision 4.7.2 (Carl Zeiss Imaging Solutions GmbH). The number of sprouts on each bead were counted using NIH ImageJ.

Oxygen-induced retinopathy

OIR was performed as described by Smith et al. (1994) and quantified according to the method of Connor et al. (2009). C57BL/6 and Pak1$^{-/-}$ mice pups (P7) with dams were exposed to 75% oxygen for 5 days and then returned to normal air at P12. Mice pups of the same age kept in normal air were used as controls. Mice pups were killed at P17 and eyes were enucleated and fixed in 4% (w/v) paraformaldehyde for 1 h at room temperature. Retinas were isolated, stained with isolectin B4, flat mounted, placed under a coverslip, and examined with a Zeiss inverted fluorescence microscope (AxioVision AX10). Retinal vasculature and neovascularization were quantified by using Nikon NIS-Elements software version AR 3.1. Retinal vasculature was calculated by determining the ratio of fluorescence intensity to total retinal area. Retinal neovascularization was quantified by first setting a

Journal of Cell Science (2016) 129, 1234-1249 doi:10.1242/jcs.179382

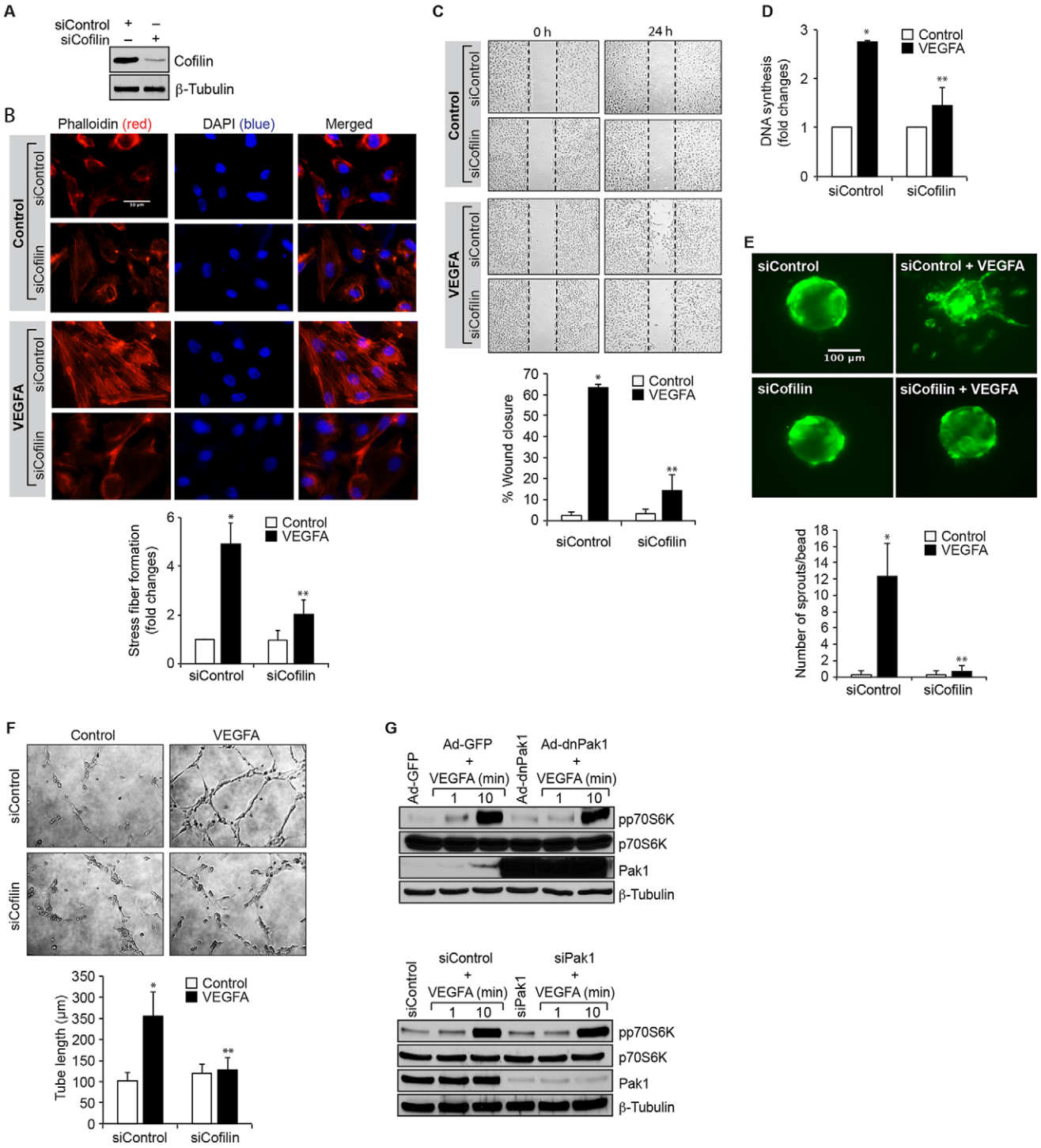

Fig. 7. Downregulation of cofilin levels inhibit VEGFA-induced angiogenic events in HRMVECs. (A) Cells were transfected with control siRNA (siControl) or cofilin siRNA (siCofilin) and 36 h later cell extracts were prepared and analyzed by western blotting for cofilin and β-tubulin levels to show the efficacy of the siRNA on its target and off target molecules. (B–F) Cells were transfected with control or cofilin siRNA, growth-arrested and subjected to VEGFA (40 ng/ml)-induced F-actin stress fiber formation (B, scale bars: 50 µm), migration (C), DNA synthesis (D), sprouting (E) or tube formation (F) assays. (G) Cells were transduced with Ad-GFP or Ad-dnPak1 (40 MOI) or transfected with siControl or siPak1, allowed to become quiescent, and treated with and without VEGFA (40 ng/ml) for the indicated time periods. Then cell extracts were prepared. Equal amounts of protein from control and each treatment were analyzed by western blotting for phosphorylated (p)p70S6K and the blots were reprobed for p70S6K, Pak1 or β-tubulin levels to show either the overexpression, knockdown or normalization. The bar graphs represent quantitative analysis of three independent experiments. The values represent mean±s.d. **P*<0.01 vs siControl; ***P*<0.01 vs siControl+VEGFA (one-way ANOVA followed by Tukey's post-hoc test).

scale with a tolerance point of 50 based on the fluorescence intensity in screenshot using Nikon NES-Elements software version AR 3.1. Neovascularity (values above 50 pixel tolerance set point) was highlighted in red and then quantified by dividing the fluorescence intensity in the highlighted area by the total fluorescence intensity in the screenshot (n=6 eyes).

Journal of Cell Science (2016) 129, 1234-1249 doi:10.1242/jcs.179382

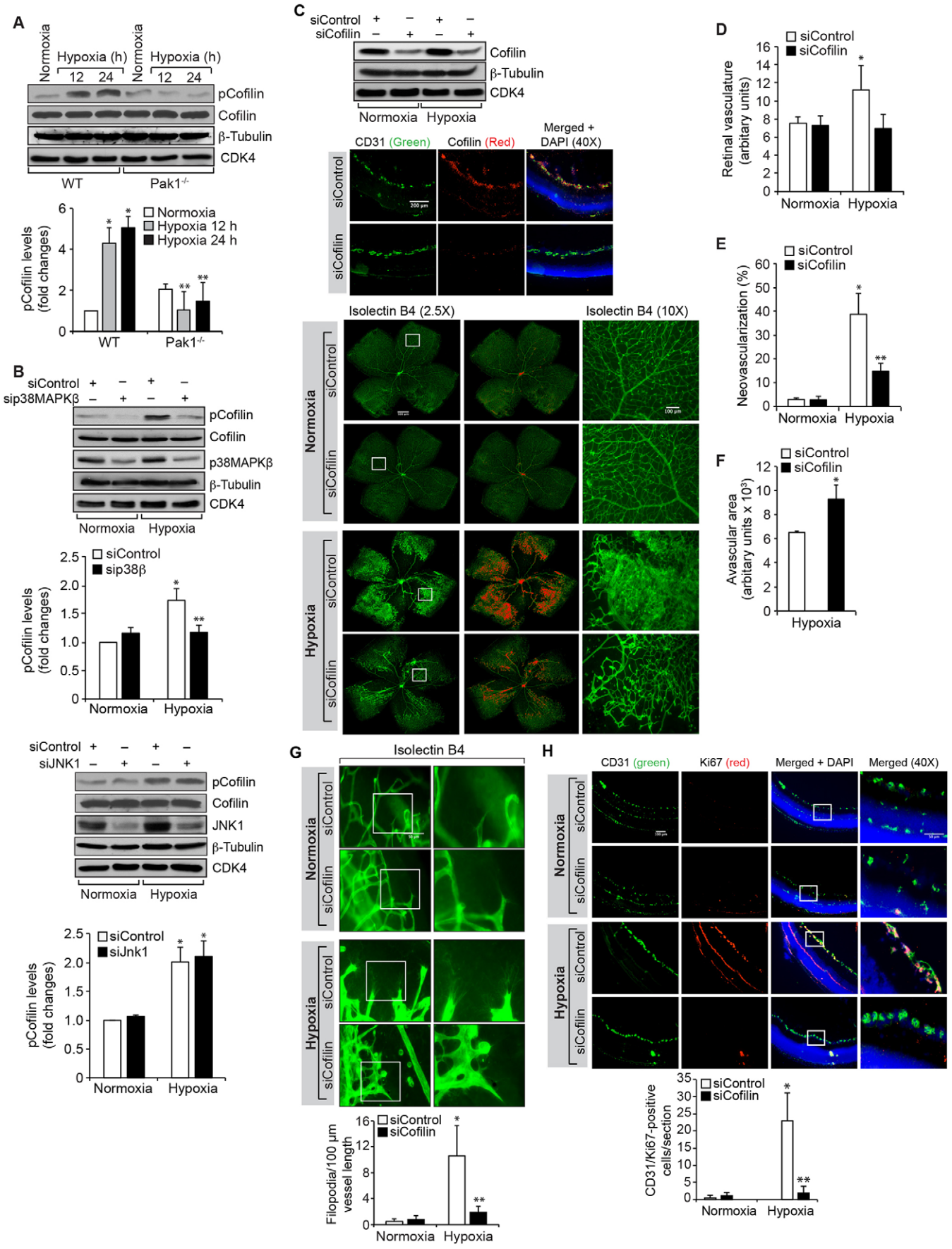

Fig. 8. See next page for legend.

Fig. 8. Downregulation of cofilin levels blocks hypoxia-induced retinal neovascularization. (A) An equal amount of protein from normoxic and various time periods of hypoxic retinal extracts was analyzed by western blotting for phosphorylated (p)cofilin levels using its phosphospecific antibodies. (B) All the conditions were the same as in A, except that the WT mice pups were injected intravitreally with control, p38MAPKβ or JNK1 siRNA (siControl, sip38MAPKβ and siJNK1, respectively) at P10, P11 and P13, the retinas were isolated. Then, extracts were prepared and analyzed by western blotting for phosphorylated cofilin levels using its phosphospecific antibodies. The blots in A and B were reprobed for cofilin, p38MAPKβ, JNK1, β-tubulin or CDK4 levels for normalization or to show the target and off-target effects of the indicated siRNA. (C) WT mice pups after exposure to 75% oxygen from P7 to P12 were injected intravitreally with control or cofilin siRNA at P12, P13 and P15. At P15 the retinas were isolated and either tissue extracts were prepared and analyzed by western blotting for cofilin, β-tubulin or CDK4 levels (to show the efficacy of the siRNA on its target and off target molecules), or fixed, cut sections were stained for CD31 and cofilin to show the effect of the siRNA on its target molecule level in endothelial cells. Alternatively, at P17 the retinas were isolated, stained with isolectin B4, and flat mounts were prepared and examined under a fluorescent microscope for retinal neovascularization. Retinal vascularization is shown in the first column. Neovascularization is highlighted in red in the second column. The third column shows the selected rectangular areas of the images in the first column under 10× magnification. (D–F) Retinal vasculature (D), neovascularization (E) and avascular area (F) were determined as described in the Materials and Methods. (G) All the conditions were the same as in C except that WT mice pups were injected intravitreally with control or cofilin siRNA at P12 and P13, and at P15 the retinas were isolated, stained with isolectin B4, and flat mounts were made and examined for filopodia. (H) All the conditions were the same as in C except that at P15 retinas were isolated, fixed, cross-sections made and stained for immunofluorescence analysis of CD31 and Ki67. The right column shows the higher magnification (as viewed at 40× magnification) of the areas selected by the rectangular boxes in the left column images. The bar graphs represent quantitative analysis of three experiments with two retinas for each. The values represent mean±s.d. **P*<0.01 vs siControl normoxia; ***P*<0.01 vs siControl hypoxia. Scale bars: 100 µm (10× images), 50 µm (40× images).

Intravitreal injections

After exposure to hyperoxia, pups were administered with scrambled, or the indicated siRNA at 1 µg/0.5 µl/eye) by intravitreal injections using a 33 G needle.

Immunofluorescence staining

After hyperoxia, mouse pups were returned to normal air for 3 days, after which time they were killed, eyes enucleated and fixed in optimal cutting temperature compound, and cryosections were prepared. To identify proliferating endothelial cells, after blocking in normal goat serum, the cryosections were probed with rabbit anti-mouse-Ki67 antibodies (1:100) and rat anti-mouse-CD31 antibodies (1:100) followed by incubation with Alexa-Fluor-568-conjugated goat anti-rabbit-IgG and Alexa-Fluor-488-conjugated goat anti-rat-IgG secondary antibodies. The sections were observed under a Zeiss inverted microscope (Zeiss Observer.Z1; ×40 NA 0.6 LD plan-Neofluar or ×10 NA 0.45 plan-Apochromat objective) and the fluorescence images were captured by a Zeiss AxioCam MRm camera using the microscope operating and image analysis software AxioVision 4.7.2 (Carl Zeiss Imaging Solutions GmbH). The retinal endothelial cell proliferation was quantified by counting Ki67- and CD31-positive cells that extended anterior to the inner limiting membrane per section (n=6 eyes, three sections/eye).

Retinal tip cell sprouting

After exposure of mice pups (P7) with 75% oxygen for 5 days, pups were returned to normal air and administered with control siRNA, p38MAPKβ siRNA or cofilin1 siRNA (1 µg/0.5 µl/eye) at P12 and P13 by intravitreal injections. Mice pups were killed at P15, eyes were enucleated and fixed in 4% (w/v) paraformaldehyde for 1 h at room temperature. Retina from fixed enucleated eyes were isolated, permeabilized with 0.5% Triton X-100, stained with Isolectin B4, flat mounted and examined under a Zeiss inverted fluorescence microscope (Zeiss Observer.Z1) at 400× magnification. Tip cells were examined at minimum 15 microscopic fields and expressed as number of filopodia/100 µm area.

Statistics

All the experiments were repeated three times and data are presented as mean±s.d. The treatment effects were analyzed by one-way ANOVA followed by Tukey's post-hoc test and the P<0.05 were considered statistically significant.

Competing interests

The authors declare no competing or financial interests.

Author contributions

R.K. performed cell migration and DNA synthesis assays, flat mount preparation, immunohistochemistry, immunofluorescence staining, retinal neovascularization, sprouting assay, tube formation assay, western blot analysis and wrote the draft manuscript; J.J. performed the actin polymerization assay; N.K.S. performed the sprouting and contributed towards drafting the manuscript; G.N.R. conceived the overall scope of the project, interpreted the data and wrote the manuscript.

Funding

This work was supported by the National Eye Institute of National Institutes of Health [grant number EY014856 to G.N.R.]. Deposited in PMC for release after 12 months.

References

Adams, R. H. and Alitalo, K. (2007). Molecular regulation of angiogenesis and lymphangiogenesis. *Nat. Rev. Mol. Cell Biol.* **8**, 464-478.
Aiello, L. P. (2005). Angiogenic pathways in diabetic retinopathy. *N. Engl. J. Med.* **353**, 839-841.
Arden, G. B. and Sivaprasad, S. (2011). Hypoxia and oxidative stress in the causation of diabetic retinopathy. *Curr. Diabetes Rev.* **7**, 291-304.
Arias-Romero, L. E. and Chernoff, J. (2008). A tale of two Paks. *Biol. Cell.* **100**, 97-108.
Beeser, A., Jaffer, Z. M., Hofmann, C. and Chernoff, J. (2005). Role of group A p21-activated kinases in activation of extracellular-regulated kinase by growth factors. *J. Biol. Chem.* **280**, 36609-36615.
Bokoch, G. M. (2003). Biology of the p21-activated kinases. *Annu. Rev. Biochem.* **72**, 743-781.
Breitsprecher, D., Koestler, S. A., Chizhov, I., Nemethova, M., Mueller, J., Goode, B. L., Small, J. V., Rottner, K. and Faix, J. (2011). Cofilin cooperates with fascin to disassemble filopodial actin filaments. *J. Cell Sci.* **124**, 3305-3318.
Carmeliet, P. (2000). Mechanisms of angiogenesis and arteriogenesis. *Nat. Med.* **6**, 389-395.
Carmeliet, P. (2003). Angiogenesis in health and disease. *Nat. Med.* **9**, 653-660.
Carmeliet, P. (2005). Angiogenesis in life, disease and medicine. *Nature* **438**, 932-936.
Connor, K. M., Krah, N. M., Dennison, R. J., Aderman, C. M., Chen, J., Guerin, K. I., Sapieha, P., Stahl, A., Willett, K. L. and Smith, L. E. H. (2009). Quantification of oxygen-induced retinopathy in the mouse: a model of vessel loss, vessel regrowth and pathological angiogenesis. *Nat. Protoc.* **4**, 1565-1573.
Dechert, M. A., Holder, J. M. and Gerthoffer, W. T. (2001). p21-activated kinase 1 participates in tracheal smooth muscle cell migration by signaling to p38 MAPK. *Am. J. Physiol. Cell Physiol.* **281**, C123-C132.
Delorme, V., Machacek, M., DerMardirossian, C., Anderson, K. L., Wittmann, T., Hanein, D., Waterman-Storer, C., Danuser, G. and Bokoch, G. M. (2007). Cofilin activity downstream of Pak1 regulates cell protrusion efficiency by organizing lamellipodium and lamella actin networks. *Dev. Cell.* **13**, 646-662.
Dharmawardhane, S., Sanders, L. C., Martin, S. S., Daniels, R. H. and Bokoch, G. M. (1997). Localization of p21-activated kinase 1 (PAK1) to pinocytic vesicles and cortical actin structures in stimulated cells. *J. Cell Biol.* **138**, 1265-1278.
Dummler, B., Ohshiro, K., Kumar, R. and Field, J. (2009). Pak protein kinases and their role in cancer. *Cancer Metastasis Rev.* **28**, 51-63.
Folkman, J. (1995). Angiogenesis in cancer, vascular, rheumatoid and other disease. *Nat. Med.* **1**, 27-30.
Garvalov, B. K., Flynn, K. C., Neukirchen, D., Meyn, L., Teusch, N., Wu, X., Brakebusch, C., Bamburg, J. R. and Bradke, F. (2007). Cdc42 regulates cofilin during the establishment of neuronal polarity. *J. Neurosci.* **27**, 13117-13129.
Gerber, H.-P., Dixit, V. and Ferrara, N. (1998). Vascular endothelial growth factor induces expression of the antiapoptotic proteins Bcl-2 and A1 in vascular endothelial cells. *J. Biol. Chem.* **273**, 13313-13316.
Gerhardt, H., Golding, M., Fruttiger, M., Ruhrberg, C., Lundkvist, A., Abramsson, A., Jeltsch, M., Mitchell, C., Alitalo, K., Shima, D. et al. (2003). VEGF guide angiogenic sprouting utilizing endothelial tip cell filopodia. *J. Cell Biol.* **161**, 1163-1177.

Ghosh, M., Song, X., Mouneimne, G., Sidani, M., Lawrence, D. S. and Condeelis, J. S. (2004). Cofilin promotes actin polymerization and defines the direction of cell motility. *Science* **304**, 743-746.
Hedges, J. C., Dechert, M. A., Yamboliev, I. A., Martin, J. L., Hickey, E., Weber, L. A. and Gerthoffer, W. T. (1999). A role for p38(MAPK)/HSP27 pathway in smooth muscle cell migration. *J. Biol. Chem.* **274**, 24211-24219.
Hellström, M., Phng, L.-K., Hofmann, J. J., Wallgard, E., Coultas, L., Lindblom, P., Alva, J., Nilsson, A.-K., Karlsson, L., Gaiano, N. et al. (2007). Dll4 signalling through Notch1 regulates formation of tip cells during angiogenesis. *Nature* **445**, 776-780.
Hellström, A., Smith, L. E. H. and Dammann, O. (2013). Retinopathy of prematurity. *Lancet* **382**, 1445-1457.
Ho, H., Soto Hopkin, A., Kapadia, R., Vasudeva, P., Schilling, J. and Ganesan, A. K. (2013). RhoJ modulates melanoma invasion by altering actin cytoskeletal dynamics. *Pigment Cell Melanoma Res.* **26**, 218-225.
Hood, J. D., Frausto, R., Kiosses, W. B., Schwartz, M. A. and Cheresh, D. A. (2003). Differential alphav integrin-mediated Ras-ERK signaling during two pathways of angiogenesis. *J. Cell Biol.* **162**, 933-943.
Hotulainen, P., Paunola, E., Vartiainen, M. K. and Lappalainen, P. (2005). Actin-depolymerizing factor and cofilin-1 play overlapping roles in promoting rapid F-actin depolymerization in mammalian nonmuscle cells. *Mol. Biol. Cell.* **16**, 649-664.
Hu, G. D., Chen, Y. H., Zhang, L., Tong, W. C., Cheng, Y. X., Luo, Y. L., Cai, S. X. and Zhang, L. (2011). The generation of the endothelial specific cdc42-deficient mice and the effect of cdc42 deletion on the angiogenesis and embryonic development. *Chin. Med. J.* **124**, 4155-4159.
Jakobsson, L., Franco, C. A., Bentley, K., Collins, R. T., Ponsioen, B., Aspalter, I. M., Rosewell, I., Busse, M., Thurston, G., Medvinsky, A. et al. (2010). Endothelial cells dynamically compete for the tip cell position during angiogenic sprouting. *Nat. Cell Biol.* **12**, 943-953.
Ke, Y., Wang, L., Pyle, W. G., de Tombe, P. P. and Solaro, R. J. (2004). Intracellular localization and functional effects of p21-activated kinase-1 (pak1) in cardiac myocytes. *Circ. Res.* **94**, 194-200.
Kichina, J. V., Goc, A., Al-Husein, B., Somanath, P. R. and Kandel, E. S. (2010). PAK1 as a therapeutic target. *Expert. Opin. Ther. Targets* **14**, 703-725.
Kim, J., Oh, W.-J., Gaiano, N., Yoshida, Y. and Gu, C. (2011). Semaphorin 3E-Plexin-D1 signaling regulates VEGF function in developmental angiogenesis via a feedback mechanism. *Genes Dev.* **25**, 1399-1411.
Kiosses, W. B., Hood, J., Yang, S., Gerritsen, M. E., Cheresh, D. A., Alderson, N. and Schwartz, M. A. (2002). A dominant-negative p65 PAK peptide inhibits angiogenesis. *Circ Res.* **90**, 697-702.
Kiuchi, T., Ohashi, K., Kurita, S. and Mizuno, K. (2007). Cofilin promotes stimulus-induced lamellipodium formation by generating an abundant supply of actin monomers. *J. Cell Biol.* **177**, 465-476.
Kundumani-Sridharan, V., Singh, N. K., Kumar, S., Gadepalli, R. and Rao, G. N. (2013). Nuclear factor of activated T cells c1 mediates p21-activated kinase 1 activation in the modulation of chemokine-induced human aortic smooth muscle cell F-actin stress fiber formation, migration, and proliferation and injury-induced vascular wall remodeling. *J. Biol. Chem.* **288**, 22150-22162.
Liu, Z., Zhang, C., Dronadula, N., Li, Q. and Rao, G. N. (2005). Blockade of nuclear factor of activated T cells activation signaling suppresses balloon injury-induced neointima formation in a rat carotid artery model. *J. Biol. Chem.* **280**, 14700-14708.
Liu, J., Fraser, S. D., Faloon, P. W., Rollins, E. L., Vom Berg, J., Starovic-Subota, O., Laliberte, A. L., Chen, J.-N., Serluca, F. C. and Childs, S. J. (2007). A betapix pak2a signaling pathway regulates cerebral vascular stability in zebrafish. *Proc. Natl. Acad. Sci. USA* **104**, 13990-13995.
Madak-Erdogan, Z., Ventrella, R., Petry, L. and Katzenellenbogen, B. S. (2014). Novel roles for ERK5 and cofilin as critical mediators linking ERα-driven transcription, actin reorganization, and invasiveness in breast cancer. *Mol. Cancer Res.* **12**, 714-727.
Mechoulam, H. and Pierce, E. A. (2003). Retinopathy of prematurity: molecular pathology and therapeutic strategies. *Am. J. Pharmacogenomics* **3**, 261-277.
Nakatsu, M. N. and Hughes, C. C. W. (2008). An optimized three-dimensional in vitro model for the analysis of angiogenesis. *Methods Enzymol.* **443**, 65-82.
Nguyen, D.-H. T., Stapleton, S. C., Yang, M. T., Cha, S. S., Choi, C. K., Galie, P. A. and Chen, C. S. (2013). Biomimetic model to reconstitute angiogenic sprouting morphogenesis in vitro. *Proc. Natl. Acad. Sci. USA* **110**, 6712-6717.
Ong, C. C., Jubb, A. M., Jakubiak, D., Zhou, W., Rudolph, J., Haverty, P. M., Kowanetz, M., Yan, Y., Tremayne, J., Lisle, R. et al. (2013). P21-activated kinase 1 (PAK1) as a therapeutic target in BRAF wild-type melanoma. *J. Natl. Cancer Inst.* **105**, 606-607.
Pierce, E. A., Avery, R. L., Foley, E. D., Aiello, L. P. and Smith, L. E. (1995). Vascular endothelial growth factor/vascular permeability factor expression in a mouse model of retinal neovascularization. *Proc. Natl. Acad. Sci. USA* **92**, 905-909.
Potente, M., Gerhardt, H. and Carmeliet, P. (2011). Basic and therapeutic aspects of angiogenesis. *Cell* **146**, 873-887.
Radu, M., Semenova, G., Kosoff, R. and Chernoff, J. (2014). PAK signalling during the development and progression of cancer. *Nat. Rev. Cancer* **14**, 13-25.
Rajashekhar, G., Kamocka, M., Marin, A., Suckow, M. A., Wolter, W. R., Badve, S., Sanjeevaiah, A. R., Pumiglia, K., Rosen, E. and Clauss, M. (2011). Pro-inflammatory angiogenesis is mediated by p38 MAP kinase. *J. Cell. Physiol.* **226**, 800-808.
Sells, M. A., Knaus, U. G., Bagrodia, S., Ambrose, D. M., Bokoch, G. M. and Chernoff, J. (1997). Human p21-activated kinase (Pak1) regulates actin organization in mammalian cells. *Curr. Biol.* **7**, 202-210.
Singh, N. K., Hansen, D. E.III, Kundumani-Sridharan, V. and Rao, G. N. (2013). Both Kdr and Flt1 play a vital role in hypoxia-induced Src-PLD1-PKCgamma-cPLA(2) activation and retinal neovascularization. *Blood* **121**, 1911-1923.
Slack-Davis, J. K., Eblen, S. T., Zecevic, M., Boerner, S. A., Tarcsafalvi, A., Diaz, H. B., Marshall, M. S., Weber, M. J., Parsons, J. T. and Catling, A. D. (2003). PAK1 phosphorylation of MEK1 regulates fibronectin-stimulated MAPK activation. *J. Cell Biol.* **162**, 281-291.
Smith, L. E., Wesolowski, E., McLellan, A., Kostyk, S. K., D'Amato, R., Sullivan, R. and D'Amore, P. A. (1994). Oxygen-induced retinopathy in the mouse. *Invest. Ophthalmol. Vis. Sci.* **35**, 101-111.
Smith, L. E., Hard, A.-L. and Hellström, A. (2013). The biology of retinopathy of prematurity: how knowledge of pathogenesis guides treatment. *Clin. Perinatol.* **40**, 201-214.
Srinivasan, R., Zabuawala, T., Huang, H., Zhang, J., Gulati, P., Fernandez, S., Karlo, J. C., Landreth, G. E., Leone, G. and Ostrowski, M. C. (2009). Erk1 and Erk2 regulate endothelial cell proliferation and migration during mouse embryonic angiogenesis. *PLoS ONE* **4**, e8283.
Sumi, T., Matsumoto, K., Takai, Y. and Nakamura, T. (1999). Cofilin phosphorylation and actin cytoskeletal dynamics regulated by rho- and Cdc42-activated LIM-kinase 2. *J. Cell Biol.* **147**, 1519-1532.
Tan, W., Palmby, T. R., Gavard, J., Amornphimoltham, P., Zheng, Y. and Gutkind, J. S. (2008). An essential role for Rac1 in endothelial cell function and vascular development. *FASEB J.* **22**, 1829-1838.
Xiao, G.-H., Beeser, A., Chernoff, J. and Testa, J. R. (2002). p21-activated kinase links Rac/Cdc-42 signaling to merlin. *J. Biol. Chem.* **277**, 883-886.
Yancopoulos, G. D., Davis, S., Gale, N. W., Rudge, J. S., Wiegand, S. J. and Holash, J. (2000). Vascular-specific growth factors and blood vessel formation. *Nature* **407**, 242-248.
Zipfel, P. A., Bunnell, S. C., Witherow, D. S., Gu, J. J., Chislock, E. M., Ring, C. and Pendergast, A. M. (2006). Role for the Abi/wave protein complex in T cell receptor-mediated proliferation and cytoskeletal remodeling. *Curr. Biol.* **16**, 35-46.